Vortex Dynamics Analysis of Unsteady Vortex Wakes

P. Sundaram*
Vigyan, Inc., Hampton, Virginia
and
M. Kurosaka† and J. M. Wu‡
University of Tennessee Space Institute, Tullahoma, Tennessee

An incompressible inviscid unsteady vortex dynamics analysis is presented to investigate the flow details for a class of free and bounded shear flows. Using the unsteady vortex models developed for the starting vortex behind sharp edges and the vortex street wakes, particle dynamics computations have been carried out to determine the pathline and streakline patterns in each of these model flows. Based on these results, the energy equation has been integrated along particle paths. The computations reconfirm that an instantaneous separation of energy occurs in the wake. Another interesting phenomenon, termed the Eckert-Weise effect, where the near-wake region contains essentially a cold flow, has also been computationally reobtained using the present vortex model. Using a similar model, the wall-bounded vortex street wake problem has also been studied. The computed results highlight the important dynamical effects of convecting unsteady vortex motion close to a wall, which indicates that the inviscid entrainment effects play a vital role on the wall layer fluid eruption.

Introduction

OUR earlier work,[1] treats the unsteady vortex motion with emphasis placed on the study of streaklines and pathlines in simple wake flows. By computing the pathlines and streaklines using inviscid vortex models, it was shown, therein, that the illusions created by a naive observation of streaklines alone can be obliviated by the simultaneous study of both streaklines and pathlines. In the present paper, we pursue this theme to investigate the important properties characteristic of vortex-dominated flows.

In Ref. 2, physical arguments were presented to show that the unsteady vortex motion in the wake is the primary cause of the instantaneous energy separation in the wake. In addition, experimental evidence and computational results, the latter obtained by solving the laminar compressible Navier-Stokes equations at low subsonic Mach numbers, verified the existence of hot and cold spots in the wake. Here, we revisit this problem and re-examine the kinematics of the flow from the present spirit of chasing fluid particles and evaluating the changes in total temperature along their trajectories.

A pathline, defined by the equation $dX/dt = U(X,t)$, is the path of a fluid particle. The pathline could be used to determine the instantaneous behavior of the flow properties at a given point lying on the locus of the particle. A streakline, given by $X = X(X_0,t,\tau)$; $\tau \leq t$, with the initial condition that $X = X_0$ at $t = \tau$ represents the instantaneous position of all fluid particles that started from a fixed point in space up to that particular instant of time. The total temperature distribution displayed at points along all the streaklines yields the instantaneous picture of the energy in the flowfield. To compute the total temperature distributions, the energy or total temperature equation has to be integrated along the particle paths of each fluid particle.

An immediate consequence of this phenomenon of energy redistribution in the wake is the aerodynamic cooling of the wake, experimentally observed by Eckert and Weise[3] more than 40 years ago. In a recent article, Eckert[4] (see also Ref. 5) rekindled the importance of energy separation in different vortex dominated flows and explained techniques of exploiting this energy separation in various flow machines. As demonstrated previously in Ref. 2, it will be shown later, by temporally averaging the instantaneous total temperature distribution obtained from following the fluid particles, that this aerodynamic cooling of the wake is a consequence of the instantaneous energy separation in the wake. This aerodynamic cooling is not special to wakes alone, but is also true for vortical structures prevalent in jets as well. Hence, by employing active methods of exciting these free shear layers, thus strengthening the shear layer vortices, very efficient convective cooling of many flow machinery components could be achieved.

The next important study undertaken using the present unsteady vortex model is the wall-bounded vortex street wake flow. A simple inviscid model for this problem was developed over half a century ago by Rosenhead.[6] This model has been extended herein to incorporate the unsteady effects. Only uniform freestream flows have been considered in the present study; the effects of wall boundary layers have also been ignored from the present model. We will present the results of the computed streaklines pattern, which clearly indicate that the streaklines that resemble secondary vortices emanating from the wall are primarily due to the entrainment effects of the convecting unsteady vortices close to the wall.

Pathlines and Streaklines

In an unsteady flow, the knowledge of fluid-particle trajectories is useful in correctly interpreting flow visualization pictures. Indeed, if a suitable dynamical model could be developed to represent the flow under investigation; the particle tracking is reduced to solving a system of nonlinear ordinary differential equations in two or three dimensions. Typical of these models are 1) a single inviscid vortex, 2) the vortex street model for the wake flow, and 3) the single vortex row approach to represent the mixing layer between two streams of unequal velocities or densities. Some examples of streakline and pathline patterns for cases 1 and 2 have been presented in Ref. 1. Here, we offer another example for case 3 and additional results for case 2.

Single Row of Vortices

The classical single row of infinite vortices is considered as the first case for the present streakline study. This vortex

Received Dec. 15, 1988; revision received Jan. 16, 1990.

*Research Engineer. Member AIAA.
†Currently at University of Washington, Seattle, WA. Associate Fellow AIAA.
‡B. H. Goethert Prof. of Aerospace Engineering. Associate Fellow AIAA.

configuration can be considered as a model for the initial stages of the mixing layer that develops between two streams of unequal velocities. The particle-path equation for this problem may be written in terms of nondimensional variables as

$$\frac{dz}{dt} = 1 - \frac{i\gamma}{2aU_s}\cot[\pi(\bar{z} - t)] \tag{1}$$

In Eq. (1), z is a complex number, U_s is the mean convection velocity of the vortex row in which the vortices are at a distance a apart, and γ is the strength of the vortices in the row. All quantities with an overbar represent complex conjugates. To integrate the preceding pathline equation and all the subsequent ones, a sixth-order Runge-Kutta-Fehlberg[7] scheme with a seventh-order error criterion for step size control has been utilized. Also, the time between successive particle release has been maintained to be very small, thus enabling an accurate and wiggle-free pathline trace that subsequently yields a smooth streakline pattern. The streakline pattern for this simulated plane mixing layer is shown in Fig. 1a, which very much resembles Fig. 1b (a photograph taken from Ref. 8). We note that the velocities induced by these vortices at large lateral distances become $U_s \pm (\gamma/2a)$, respectively, which represents a shear flow as a freestream. Note also that the turning points discussed in Ref. 1 do appear in a single row of vortices as well.

Double Row of Vortices

The complex potential for the Kármán's infinite double row of staggered vortices superposed on a uniform onset flow U_∞ is written (see Ref. 9) in a vortex fixed coordinate system as

$$W(z) = U_\infty z + \frac{i\gamma}{2\pi}\ell_n \sin\left[\frac{\pi}{a}\left(z - \frac{ih}{2}\right)\right] - \frac{i\gamma}{2\pi}\ell_n \sin\left[\frac{\pi}{a}\left(z - \frac{a}{2} + \frac{ih}{2}\right)\right] \tag{2}$$

where γ and $-\gamma$ are the circulation of each vortex in the top and bottom row and a and h are the longitudinal spacing between the vortices of the same row and lateral distance between opposite rows, respectively. The street moves with a uniform velocity

$$U_{st} = \frac{\gamma}{2\pi a}\tanh\left(\frac{\pi h}{a}\right)$$

Since it is intended to study the streakline pattern in a laboratory coordinate system, it is necessary to change the equations to this inertial frame of reference by superposing the vortex velocity distance $U_{st}t$. After proper nondimensionalization of the equations and denoting the nondimensional variables as the original variables, the particle path equation can be written as

$$\frac{dz}{dt} = \frac{U_\infty}{U_{st}}\left(\frac{1}{h/a} - \frac{i\gamma}{2hU_\infty}\left\{\cot\left[\frac{\pi h}{a}\left(\bar{z} - \frac{t}{h/a} + \frac{i}{2}\right)\right] - \cot\left[\frac{\pi h}{a}\left(\bar{z} - \frac{t}{h/a} - \frac{i}{2} - \frac{1}{2h/a}\right)\right]\right\}\right) \tag{3}$$

and the vortex street velocity is once again written in the laboratory coordinate system as

$$\frac{U_{st}}{U_\infty} = 1 - \frac{\gamma}{hU_\infty}\left(\frac{h}{a}\right)\tanh\left(\frac{\pi h}{a}\right) \tag{4}$$

The unknown parameters in these equations are the vortex street spacing ratio (h/a) and the nondimensional Rankine vortex circulation (γ/hU_∞). We chose these values to be 0.18 and 2.234, respectively, which correspond to the experimental data of Griffin and Ramberg[10] for a circular cylinder wake at a Reynolds number of 5×10^2. (The vortex cores were assumed to be circular and of unit nondimensional diameter.)

Solving Eq. (3) for a particular initial condition, we compute the pathline at any specific instant of time. By joining the instantaneous location of all fluid particles released from the same point at different initial time t_0 we obtain the streakline pattern at a particular time t_1. The particle release points along the y axis were chosen so as to exclude those particles that would be engulfed into these Rankine vortex cores, in accordance with the physical observation that fluid outside the core cannot enter the core. Since vortices are modeled rather than numerically captured, there is no need to analyze the numerical stability in the present computations. Figure 2a depicts the streaklines for particles released from various y locations. The computed streaklines show good comparison with the flow visualization results of Ref. 11, as shown in Fig. 2b. The computed streaklines clearly highlight two families of turning points as discussed in Ref. 1, which correspond to the relative extrema of the distance between the particle release point and the nearest vortex location. These details have also been observed for the well-known case of Kármán's vortex street with spacing ratio, $(h/a) = 0.281$. In phase space, the streaklines pattern in the neighborhood of the vortices indicate a limit-cycle-like behavior for which the vortices act like attractors, whereas the turning points behave like stable and unstable foci.

To incorporate the viscous diffusion effects on the vortex street, Schaefer and Eskinazi[12] have proposed a scheme in which they replaced the strength of each vortex in the vortex street by the Lamb-Oseen exponential decay solution

$$\gamma = \gamma_0\left[1 - \exp\left(\frac{-r^2}{4\nu t}\right)\right]$$

where γ is the strength of the vortex at time t while its initial strength was γ_0, r is the distance between the point of interest and the vortex center, and ν is the kinematic viscosity. In the present work, a similar procedure is adopted; but we differ in the technique in that a semi-infinite street of vortices with exponential decay have been substituted in the place of constant strength vortices from the original infinite Kármán street

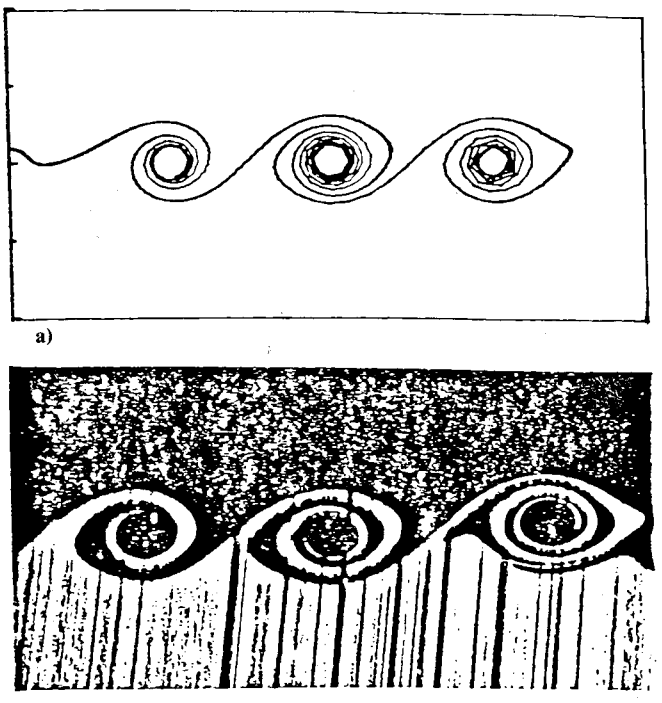

a)

b)

Fig. 1 Streakline for a plane mixing layer: a) computed and b) flow-visualization picture.[8]

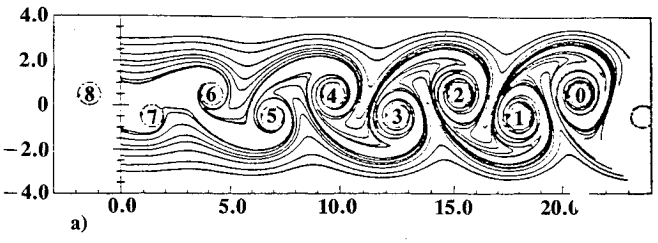

Fig. 2 Streaklines for a vortex street wake, $t_1 = 3.75$: a) computed; and b) smoke flow-visualization photograph.[11]

as they cross the y axis. After introducing yet another nondimensional variable $\nu^* = (\nu/U_{st}h)$, the particle path equation is rewritten as

$$\frac{dz}{dt} = \frac{U_\infty}{U_{st}}\left(\frac{1}{\lambda} - \frac{i}{2}\frac{\gamma}{hU_\infty}\left\{\cot\left[\frac{\pi h}{a}\left(\bar{z} - \frac{t}{\lambda} + \frac{i}{2}\right)\right] - \cot\left[\frac{\pi h}{a}\left(\bar{z} - \frac{t}{\lambda} - \frac{i}{2} - \frac{1}{2\lambda}\right)\right]\right\}\right.$$
$$+ \sigma\frac{[1 - \exp(-|z^-|^2\lambda/4\nu\tau_2)]}{z^-}$$
$$+ \sigma\sum_{n=1}^{\infty}\frac{(1 - \exp\{-|z^- - g|^2\lambda/[4\nu(n+\tau_2)]\})}{(z^- - g)}$$
$$+ \sigma\frac{1}{z^+} + \sigma\sum_{n=1}^{\infty}\frac{1}{(z^+ - [g + (\tfrac{1}{2}\lambda)])}$$
$$\left. - \sigma\frac{1}{z^-} - \sigma\sum_{n=1}^{\infty}\frac{1}{(z^- - g)}\right) \tag{5}$$

where we have replaced (h/a) by λ and $(i\gamma/2\pi\lambda hU_\infty)$ by σ for compactness and

$$z^+ = \left(z - \frac{\tau_1}{\lambda} - \frac{i}{2}\right)$$

$$z^- = \left(z - \frac{\tau_2}{\lambda} + \frac{i}{2}\right)$$

$$\text{and } g = \frac{n - \tfrac{1}{2}}{\lambda}$$

with $\tau_1(0,1) = [t - \text{int}(t)]$ and $\tau_2 = \max(0, \tau_1 - \tfrac{1}{2})$. No account for the effects of diffusion in the street velocity or the spacing ratio itself have been made because the main interest here is to evaluate the first-order diffusion effects only. As can be seen from Fig. 3, the nature of the streakline pattern computed using Eq. (5) indeed did not change significantly.

Wall-Bounded Vortex Flows

Next, let us consider the case that the wake, represented by an infinite vortex street with each vortex of constant strength $\pm\gamma$, be confined between two solid walls. The presence of the two walls can be modeled by a doubly infinite image vortex system with the vortex strengths once again being $\pm\gamma$. Early work in this area was carried out by Rosenhead[6] and Glauert[13] while considering the wind-tunnel interference problem. In the present study, we investigate the aspect of entrainment effects of the convecting wake vortices moving close to a solid wall. The study is essentially inviscid with the implicit understanding that the effect of viscosity is confined to the vortex core region and the region close to the wall.

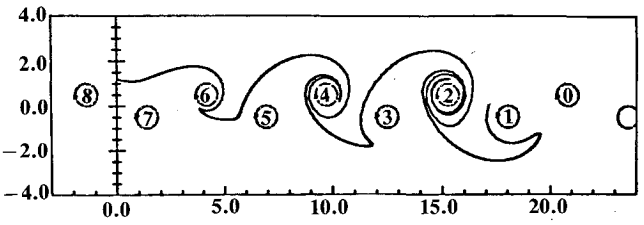

Fig. 3 Streakline in a viscous vortex street with Lamb's decaying vortices.

The complex potential for the case of an infinite Kármán vortex street bounded between two channel walls at $\pm(c/2)$ becomes

$$W = \frac{i\gamma}{2\pi}\ln\left\{\frac{\prod_{r=-\infty}^{r=\infty}\sinh\left[(\mu_1 - ra)\frac{\pi}{2c}\right]}{\prod_{r=-\infty}^{r=\infty}\cosh\left[(\mu_2 - ra)\frac{\pi}{2c}\right]}\right.$$
$$\left.\times\frac{\prod_{s=-\infty}^{s=\infty}\cosh\left[\left(\mu_1 - sa + \frac{a}{2}\right)\frac{\pi}{2c}\right]}{\prod_{s=-\infty}^{s=\infty}\sinh\left[\left(\mu_2 + sa + \frac{a}{2}\right)\frac{\pi}{2c}\right]}\right\}$$

where the product over r represents the contributions from all positive vortices and that over s represents the contributions from all negative vortices; μ_1 and μ_2 represent $(z - ih/2)$ and $(z + ih/2)$, respectively. With the infinite sum replaced by a semi-infinite sum and using the product formula for the hyperbolic functions and then letting

$$q_1 = \exp\left(-\frac{\pi a}{2c}\right), \qquad \tau_1 = 2ic$$

we obtain

$$W = \frac{i\gamma}{2\pi}\ln\left\{\frac{\sin\frac{\mu_1\pi}{\tau}\prod_{r=1}^{r=\infty}\left(1 - 2q_1^{2r}\cos\frac{2\mu_1\pi}{\tau} + q_1^{4r}\right)}{\cos\frac{\mu_2\pi}{\tau}\prod_{r=1}^{r=\infty}\left(1 + 2q_1^{2r}\cos\frac{2\mu_2\pi}{\tau} + q_1^{4r}\right)}\right.$$
$$\left.\times\frac{\prod_{s=1}^{s=\infty}\left(1 + 2q_1^{2s-1}\cos\frac{2\mu_1\pi}{\tau} + q_1^{4s-2}\right)}{\prod_{s=1}^{s=\infty}\left(1 - 2q_1^{2s-1}\cos\frac{2\mu_2\pi}{\tau} + q_1^{4s-2}\right)}\right\} \tag{6}$$

This is the complex velocity potential for a wall-bounded vortex street in a coordinate system moving with a vortex.

To find the complex potential in a laboratory coordinate system, we need to displace the coordinates by the quantity $-U_{st}^b t$ to all z positions in Eq. (6), where U_{st}^b is the velocity of the wall-bounded vortex street in the positive x direction. Using the substitution,

$$\xi = (\pi/\tau)(\mu_1 - U_{st}^b), \qquad \eta = (\pi/\tau)(\mu_2 - U_{st}^b)$$

Eq. (6) becomes

$$W = \frac{i\gamma}{2\pi} \ell n \left\{ \frac{\sin\xi \prod_{r=1}^{r=\infty} (1 - 2q_1^{2r}\cos 2\xi + q_1^{4r})}{\cos\eta \prod_{r=1}^{r=\infty} (1 + 2q_1^{2r}\cos 2\eta + q_1^{4r})} \times \frac{\prod_{s=1}^{s=\infty} (1 + 2q_1^{2s-1}\cos 2\xi + q_1^{4s-2})}{\prod_{s=1}^{s=\infty} (1 - 2q_1^{2s-1}\cos 2\eta + q_1^{4s-2})} \right\} \tag{7}$$

Thus, the equation for the particle path is given by

$$\frac{dz}{dt} = \frac{U_\infty}{U_{st}^b d}\left(1 + \left(\frac{\gamma}{2cU_\infty}\right)\left\{\sum_{j=1}^{\infty} 2q_1^{2j-1}\left[\sin 2\bar{\xi}\left(\frac{q_1\overline{V_2} - \overline{V_1}}{\overline{V_1}V_2}\right) + \sin 2\bar{\eta}\left(\frac{q_1\overline{V_4} - \overline{V_3}}{\overline{V_3}\,\overline{V_4}}\right)\right] + \frac{1}{2}(\tan\bar{\eta} + \cot\bar{\xi})\right\}\right) \tag{8}$$

where

$$\overline{V_1} = \left(1 - 2q_1^{2j}\cos 2\bar{\xi} + q_1^{4j}\right)$$
$$\overline{V_2} = \left(1 + 2q_1^{2j-1}\cos 2\bar{\xi} + q_1^{4j-2}\right)$$
$$\overline{V_3} = \left(1 + 2q_1^{2j}\cos 2\bar{\eta} + q_1^{4j}\right)$$
$$\overline{V_4} = \left(1 - 2q_1^{2j-1}\cos 2\bar{\eta} + q_1^{4j-2}\right)$$

The ratio of the vortex street velocity to the freestream velocity can be derived as

$$\frac{U_{st}^b}{U_\infty} = 1 - \left(\frac{\gamma}{hU_\infty}\right)\left(\frac{d}{2}\right)\left(\tanh(\pi d) - \sum_{r=1}^{\infty}\left\{\frac{4\exp(-2\pi r d e)}{1 - [-\exp(-2\pi d e)]^r}\sinh(2\pi r d)\right\}\right) \tag{9}$$

with street height ratio $d = (h/a)$, and wall height ratio $e = (c/h)$.

Equation (8) can be expressed in terms of the Jacobian elliptic functions, and series approximations for these sums can be applied. Instead, we chose a direct approach but limit the computations to a small number of vortices. The vortex street parameters have been set to the values corresponding to the unbounded vortex street case prescribed earlier. Although the consideration of a uniform freestream is not quite correct for a channel flow where the boundary layer exists on the walls, it is a reasonable approximation for a fully developed turbulent flow in the tunnel. Streakline and pathline patterns for this wall-bounded vortex street problem have been computed based on the previous unsteady vortex model. These particles were continuously released from different y locations from $x = 0$. Figures 4a and 4b show the streakline pattern corresponding to c values of 3.0 and 6.0 at the present time $t_1 = 3.25$. The streakline patterns for the particle released close to a wall indicate the entrainment or eruption effect of the convecting vortices. The corresponding pathline pattern is given in Figs. 5a and 5b.

From the inviscid streakline computations presented in Figs. 4a and 4b and also verified by the flow visualization movie obtained from the University of Tennessee Space Institute (UTSI) water-tunnel facility, it seems almost certain that the eruption-like appearances of the near-wall streaklines is merely due to the inviscid entrainment effect of the vortices. It is reiterated here that utmost care needs to be taken while interpreting the physical motion based on the streakline observation alone.

Energy Distribution in a Vortex Street Wake

A puzzling observation that the total temperature in the wake of a bluff body can become substantially lower then the freestream value is manifested in Ref. 3, by the measurement of negative recovery factors near the rearmost surface of a bluff body at high subsonic Mach numbers. This aerodynamic cooling phenomenon, known as the Eckert-Weise effect, has recently been investigated in detail in Ref. 2, and its cause has been pinned down to be the vortex shedding from the body. In the present study (a summary of the detailed discussion given in Ref. 14), we revisit this through the method of particle tracking and show, once again, that the Eckert-Weise effect is a consequence of the energy separation phenomenon that occurs in the wake of bluff bodies.

The fundamental equation of interest is the frictionless form of the energy equation, which can be written as (see Ref. 15)

$$c_p \frac{DT_t}{Dt} = \frac{1}{\rho}\frac{\partial p}{\partial t} \tag{10}$$

where T_t is the total temperature; c_p, ρ, p, and t are the specific heat at constant pressure, density, static pressure, and time, respectively; and (D/Dt) denotes total derivative. This

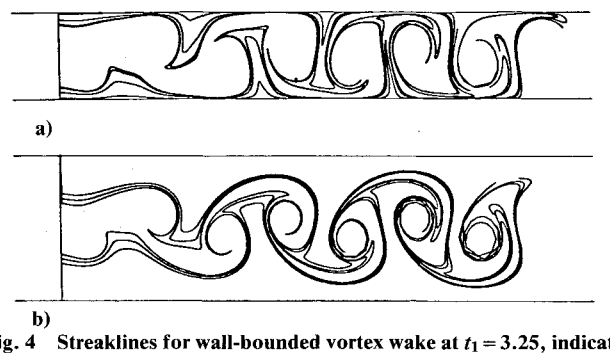

Fig. 4 Streaklines for wall-bounded vortex wake at $t_1 = 3.25$, indicating the effect of walls: a) $c/h = 3.0$, streaklines close to walls show eruption-like behavior and they switch sides; and b) $c/h = 6.0$, streaklines nearly undisturbed.

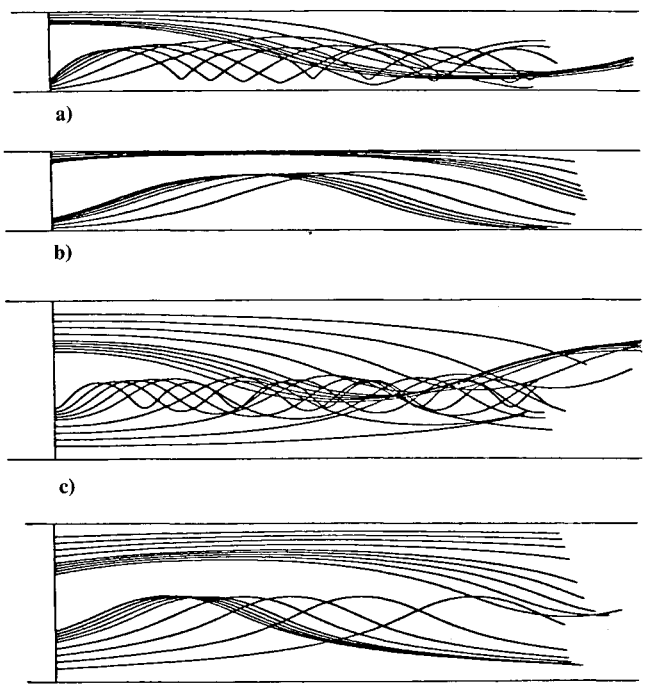

Fig. 5 Pathlines for a wall-bounded vortex wake: a) $c/h = 3.0$, $t_0 = 0.0$; b) $c/h = 3.0$, $t_0 = 0.2$; c) $c/h = 6.0$, $t_0 = 0.0$, and d) $c/h = 6.0$, $t_0 = 0.2$.

equation shows that in an inviscid unsteady flow the energy distribution at any point is proportional to the sum of the rate at which the instantaneous pressure changes have occurred over the time it takes to reach that point. It is important to realize that the unsteady nature of the flow implies that the local energy is path dependent and, hence, the integration should be carried out along particle paths.

Assuming an irrotational flow in the region outside the vortex cores, we can once again associate a velocity potential ϕ for the two-dimensional unsteady flow. The unsteady pressure term in Eq. (10) can be derived from the generalized Bernoulli equation:

$$\frac{p}{\rho}+\frac{1}{2}q^2+\frac{\partial\phi}{\partial t}=\frac{p_\infty}{\rho}+\frac{1}{2}U_\infty^2$$

where q is the resultant velocity. With $W=\phi+i\psi$ as the complex potential and $\phi=(W+\bar{W})/2$, the relation between q and W becomes

$$q^2=\frac{\mathrm{d}W}{\mathrm{d}z}\left(\overline{\frac{\mathrm{d}W}{\mathrm{d}z}}\right)$$

After some algebra, we can write the unsteady pressure term as

$$\frac{1}{\rho}\frac{\partial p}{\partial t}=-\left(\frac{1}{2}\right)\left(\frac{\gamma}{2hU_\infty}\right)\pi\left(\frac{h}{a^2}\right)U_\infty^3(\Psi+\bar{\Psi})$$

with $\Psi(t,z)$ defined as

$$\Psi=i\left(\frac{U_{\mathrm{st}}}{U_\infty}\right)\left(\frac{1}{\sin^2\Theta_1}-\frac{1}{\sin^2\Theta_2}\right)$$

$$\times\left[1-i\frac{\gamma}{2hU_\infty}\left(\frac{h}{a}\right)(\cot\bar{\Theta}_1-\cot\bar{\Theta}_2)-\left(\frac{U_{\mathrm{st}}}{U_\infty}\right)\right]$$

and

$$\Theta_1=\frac{\pi}{a}\left(z-U_{\mathrm{st}}-i\frac{h}{2}\right)$$

$$\Theta_2=\frac{\pi}{a}\left(z-U_{\mathrm{st}}-\frac{a}{2}+i\frac{h}{2}\right)$$

Substituting the previous equation for the unsteady pressure term in the energy equation, Eq. (10), it becomes of the form

$$c_p\frac{\mathrm{D}T_t}{\mathrm{D}t}=-\left(\frac{1}{2}\right)\left(\frac{\gamma}{2hU_\infty}\right)\pi\left(\frac{h}{a^2}\right)U_\infty^3(\Psi+\bar{\Psi}) \qquad (11)$$

Using the usual nondimensionalization and also introducing the nondimensional total temperature as

$$T_t^*=\frac{2c_pU_{\mathrm{st}}}{(\gamma/2hU_\infty)\pi(h/a)U_\infty^3}T_t$$

the final form of the energy equation, with the nondimensional variables and dropping the * becomes

$$\frac{\mathrm{D}T_t}{\mathrm{D}t}=-(\Psi+\bar{\Psi}) \qquad (12)$$

Integrating Eq. (12) along pathlines, the change in the total temperature between two positions over a certain time is given by the relation

$$\Delta T_t=T_t-T_{t_0}=-\int_{t_0}^{t}(\Psi+\bar{\Psi})\,\mathrm{D}t \qquad (13)$$

By fixing the total temperature of a particle at the release point as zero, the T_t values at any other point along its trajectory, determined by the solution of Eq. (3), can be computed from the previous integral equation.

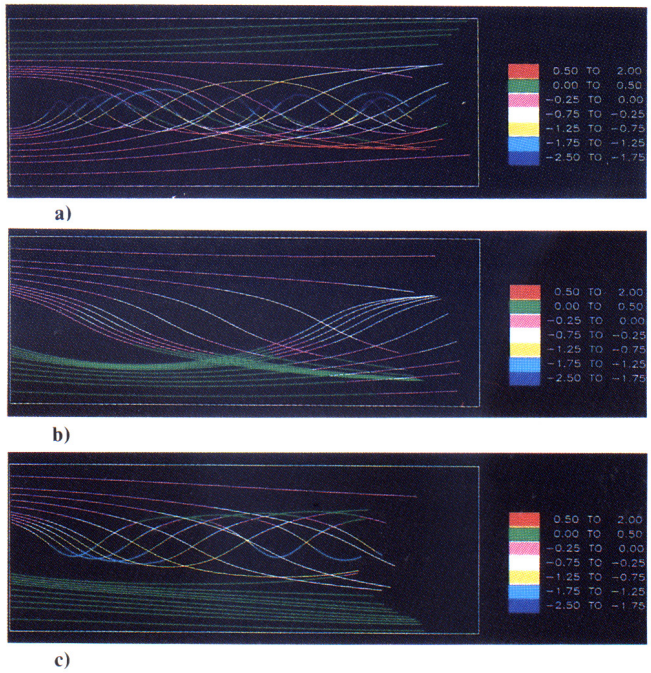

Fig. 6 Color plot showing T_t variations along pathlines at $t_1=3.75$ for various start times: a) $t_0=0.0$; b) $t_0=0.2$; and c) $t_0=0.4$.

Fig. 7 Computed streakline picture showing instantanous T_t distribution in the vortex street wake at $t_1=3.75$.

The computed T_t variation along the pathlines released at various y locations is shown in Fig. 6a–6c. Releasing of particles in Fig. 6a–6c were started at $t_0=0.0$, 0.2, and 0.4, respectively. It is important to note the significant differences in the pathline pattern and the corresponding T_t values along the pathline for various start times. The procedure for obtaining the streakline pattern and the temperature values at each point along the streakline are once again the same as just described.

A complete picture of the instantaneous total temperature distribution in the vortex street wake can be obtained by calculating the T_t values along streaklines. Figure 7 gives the color-graphics picture of the total temperature distribution in the wake at time $t=3.75$. It is clearly seen that the center portion of the wake is essentially cold and several spots of hot flow exist at the outer edges of the wake near the vortices. These results show good qualitative agreement with the numerical solution of the Navier-Stokes equations (Fig. 10, Ref. 2). The numerical results in Ref. 2 were computed at a Mach number of 0.35, whereas the present streaklines were computed based on the incompressibility assumption and so the two results cannot be directly compared. As pointed out in Ref. 2, we note that for an incompressible flow, the distribution of total temperature in the wake is equivalent to that of the total pressure.

With the energy separation in the vortex wake thus reproduced similar to Ref. 2 using the present unsteady vortex model, the temporal average of these instantaneous T_t distributions in the wake has been considered next. This study is aimed at simulating the aerodynamic cooling phenomenon described earlier. We will demonstrate here that the Eckert-Weise effect is only a time-averaged result of energy separa-

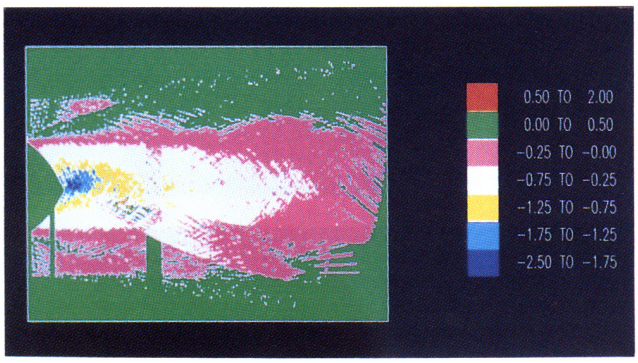

Fig. 8 Color graphics giving the temporal average of T_t distribution in the vortex street wake at $t_1 = 3.0$.

tion. The actual procedure to compute the temporal average values of T_t at each point is given in the following paragraph.

After dividing the near wake region into a fine mesh of rectangular cells, a T_t value of zero has been assigned initially to each cell corner. As a particle traverses along its path, the cell corners surrounding the particle at each instant of time has been identified. To interpolate the T_t values at the cell corners based on those values along the particle path, a Taylor series expansion around the point along the particle has been considered. Thus, as the particle traverses along its path, the indices of the vertices of the rectangular cells closest to the position of the particle, the T_t values at these cell corners, and the time of arrival of the particle at that point are all computed and stored. This sequence of steps has been carried out for each fluid particle released from the start to the final time. Thus, a set of entries (T_t) at each cell corner has been obtained. A standard sorting routine has been used to arrange the t in ascending order. Assuming that the T_t value is zero until the first fluid particle arrived at any cell, and the T_t value remains constant between the successive arrival of particles carrying different T_t values into a cell, the time averaged T_t at each cell corner has been computed.

Figure 8 is the color picture showing the time-averaged T_t distribution obtained from the instantaneous value of Fig. 7. It clearly indicates that the periodic hot spots that are apparent in the instantaneous energy distribution picture of Fig. 7 have been replaced by a colder distribution of temperatures in the entire wake. Furthermore, we can also observe that very high negative total temperature values have been obtained along the wake centerline in the near wake. This implies that temporal averaging essentially hides the independent hot and cold regions in the wake and results in the apparent depleted energy distribution throughout the interior portions of the wake. This is clearly indicative of the Eckert-Weise effect. Thus, we conclude here, as we did previously in Ref. 2, that the Eckert-Weise effect is indeed a time-averaged effect of the instantaneous energy separation that occurs in the wake.

Conclusion

In the present study, three basic unsteady flows have been investigated. The present simple unsteady vortex model is shown to be capable of capturing the kinematical features of the flow involving large scale vortex motion. The important mechanisms for the unsteady flow phenomena such as energy separation and aerodynamic cooling, which have caused considerable speculations in the past, have been reconfirmed to be due to the unsteady vortex motion only. Similar phenomena should also occur in jets.

References

[1]Kurosaka, M., and Sundaram, P., "Illustrative Examples of Streaklines in Unsteady Vortices: Interpretational Difficulties Revisited," *Physics of Fluids*, Vol. 29, No. 10, 1986, pp. 3474–3477.

[2]Kurosaka, M., et al., "Energy Separation in a Vortex Street," *Journal of Fluid Mechanics*, Vol. 176, 1987, pp. 1–29.

[3]Eckert, E. R. G., and Weise, W., "Messungen der Temperaturerteilung auf der ober Fläche Schnell Angeströmter Unbeheizter Körper," *Forschg. Ing. Wesen*, Vol. 13, 1943, pp. 246–254.

[4]Eckert, E. R. G., "Experiments on Energy Separation in Fluid Streams," *Journal of Mechanical Engineering*, Vol. 106, No. 10, 1984, pp. 58–65.

[5]Eckert, E. R. G., "Cross Transport of Energy in Fluid Streams," *Warme-und Stoffubertragung*, 21, 1987, pp. 73–81.

[6]Rosenhead L., "The Kármán Street of Vortices in a Channel of Infinite Breadth," *Philosophical Transactions of the Royal Society of London, Series A*, Vol. 228, 1929, pp. 275–329.

[7]Fehlberg, E., "Classical Fifth-, Sixth-, Seventh-, and Eighth-Order Runge-Kutta Formulas with Stepsize Control," NASA-TR R-287, 1968.

[8]Van Dyke, M., *An Album of Fluid Motion*, Parabolic, 1982.

[9]Milne-Thompson, L. M., *Theoretical Hydrodynamics*, 5th ed., MacMillan, New York, 1960.

[10]Griffin, O. M., and Ramberg, S. E., "The Vortex-Street Wakes of Vibrating Cylinders," *Journal of Fluid Mechanics*, Vol. 66, 1974, pp. 553–576.

[11]Cornish, J. J., "Vortex Flows," Eighth Quick-Goethert Lecture, Univ. of Tenn. Space Inst., 1982.

[12]Schaefer, J. W., and Eskinanzi, S., "Analysis of the Vortex Street Generated in a Viscous Fluid," *Journal of Fluid Mechanics*, Vol. 6, 1960, pp. 241–260.

[13]Glauert, H., "The Characteristics of a Kármán Vortex Street in a Channel of Finite Breadth," *Proceedings of the Royal Society of London*, A122, 1928, pp. 34–45.

[14]Sundaram, P., "Studies on Unsteady Vortex Motions Including Thermo-Fluid Interactions," Ph.D. Dissertation, Univ. of Tennessee, Tullahoma, TN, 1987.

[15]Liepmann, H. W., and Roshko, A., *Elements of Gas Dynamics*, Wiley, 1957.

Color reproductions courtesy of Vigyan, Inc. and the University of Tennessee Space Institute